Fast filtering algorithm based on vibration systems and neural information exchange and its application to micro motion robot*

Gao Wa(高 娃)[a], Zha Fu-Sheng(查富生)[a], Song Bao-Yu(宋宝玉)[b], and Li Man-Tian(李满天)[a]†

[a] State Key Laboratory of Robotics and System, Harbin Institute of Technology, Harbin 150001, China
[b] Department of Mechanical Design, Harbin Institute of Technology, Harbin 150001, China

(Received 7 March 2013; revised manuscript received 2 June 2013; published 3 December 2013)

This paper develops a fast filtering algorithm based on vibration systems theory and neural information exchange approach. The characters, including the derivation process and parameter analysis, are discussed and the feasibility and the effectiveness are testified by the filtering performance compared with various filtering methods, such as the fast wavelet transform algorithm, the particle filtering method and our previously developed single degree of freedom vibration system filtering algorithm, according to simulation and practical approaches. Meanwhile, the comparisons indicate that a significant advantage of the proposed fast filtering algorithm is its extremely fast filtering speed with good filtering performance. Further, the developed fast filtering algorithm is applied to the navigation and positioning system of the micro motion robot, which is a high real-time requirement for the signals preprocessing. Then, the preprocessing data is used to estimate the heading angle error and the attitude angle error of the micro motion robot. The estimation experiments illustrate the high practicality of the proposed fast filtering algorithm.

Keywords: fast filtering, vibration system, neural information exchange, micro motion robot

PACS: 07.50.Qx, 43.40.Cw, 07.10.Cm, 45.40.Ln **DOI:** 10.1088/1674-1056/23/1/010701

1. Introduction

The fast wavelet transform (FWT) algorithm and the particle filtering method are considered as common and effective ways for the signals acquired to be non-stationary, such as radar signals, speech signals and biological signals, etc.[1–3] However, in practice, due to different scenarios, both approaches sometimes exhibit a certain degree of unacceptable performance, especially in the limited environment of computational speed and precision.[4–6] FWT was developed by Stang,[7] Cody,[8] and Beylkin[9] based on the wavelet transform, which was first introduced by Grossmann and Morlet.[10] It considers turning waveforms or signals in the time domain to a sequence of coefficients based on an orthogonal basis of wavelets.[11] Compared with the wavelet transform, FWT has been developed to simplify computation, as shown by Refs. [7]–[10] and the references therein. Yet, unsatisfactory performance exists in some situations, e.g., in stochastic systems. On this occasion, the H_∞ filtering method was developed by Zhang *et al*. It has been proved to be effective for stochastic signals, but it brings a great computational load.[12,13] The particle filtering method, also referred to as the sequential Monte Carlo method, is a statistical model-based estimation method.[3,14] It can be used to filter various nonlinear and stochastic signals and construct the posterior probability distribution of signals based on the available measurements and the assumption of noise probability distribution.[15–17] Yet, the approximate design of posterior probability distribution is quite difficult and often enhances the complexity of computation, e.g., Refs. [16] and [18]. Recently, research objects have become more and more complex and the information load on signals shows a great increase. Accordingly, a fast filtering algorithm, which is of fast filtering speed and good filtering performance, is demanded for real paradigms, especially for embedded systems, real-time systems, etc.

In another aspect, vibration phenomena can be observed in most actual signals (e.g., speed signals, radio signals, speech signals, etc.). No matter how forms vary, the vibration systems obey the similar objective law and corresponding mathematical principle and do not depend on situations.[19–21] Thus, this provides the possibility to establish a unified filtering algorithm based on vibration theory. Besides, to introduce the adaptability and extensibility, the properties of neurons are considered.[22] With regard to the filtering mechanism of biological neurons, the essence mainly lies in the neural information exchange by synaptic depression and facilitation.[23,24] It is completely different from common filtering theories and provides an innovative way for information processing. Hence, the details aforementioned inspire us for a further study to develop a much simpler and more powerful filtering method by making use of vibration systems theory and a neural information exchange approach.

*Project supported by the National Natural Science Foundation of China (Grant Nos. 60901074, 51075092, 61005076, and 61175107), the National High Technology Research and Development Program of China (Grant No. 2007AA042105), and the Natural Science Foundation of Heilongjiang Province, China (Grant No. E200903).

†Corresponding author. E-mail: skymoon.hit@gmail.com

© 2014 Chinese Physical Society and IOP Publishing Ltd

In previous work, a single degree of freedom vibration system filtering algorithm was developed, as mentioned in Ref. [25]. Compared with the FWT algorithm and the particle filtering method, the single degree of freedom vibration system filtering algorithm provides a faster filtering speed for signals with noise, in practice. The computation time of the FWT algorithm, the particle filtering method and the single degree of freedom vibration system filtering algorithm are calculated in LPC2148 (the main frequency is 60 MHz). The results show that the filtering speed of the single degree of freedom vibration system filtering algorithm is approximately 65 and 51 times, respectively, than that of the FWT algorithm and the particle filtering method. However, it is still not quite fast enough for some real occasions, e.g., the high real-time system, such as the navigation and positioning system of micro motion robot.

Accordingly, a further research work is studied in this paper. We focus on a much faster filtering algorithm that shows higher filtering speed, lower computation and better filtering performance based on vibration systems and neural information exchange. The remainder of this paper is organized as follows. In Section 2, we describe the developed fast filtering algorithm including the derivation process and parameter analysis. We also give the kernel of the developed fast filtering algorithm and the selection rules of parameter combination. In Section 3, for evaluation purposes, we provide two sets of experiments respectively from simulation and practice. Then, the proposed fast filtering algorithm is applied to the micro motion robot, which is of high requirements of real-time processing and efficient working. In Section 4, the paper is completed with some concluding remarks.

2. Methods

2.1. Proposed fast filtering algorithm based on vibration systems and neural information exchange

Considering resonance character of vibration systems, only one resonance frequency exists for the single degree of freedom vibration system. The closer the natural frequency of vibration is relative to the external excitation, the greater the response amplitude is.[19] In a sense, it indicates that the single degree of freedom vibration system performs a filtering ability. Accordingly, taking into account a typical single degree of freedom vibration system, the mathematical expression can be described by the following second-order differential equation

$$m\ddot{x}(t)+c\dot{x}(t)+kx(t)=f(t), \tag{1}$$

where m, c, and k represent the mass, the damping coefficient, and the stiffness coefficient, respectively, $x(t)$, $\dot{x}(t)$, and $\ddot{x}(t)$ represent the displacement, the velocity and the acceleration of the single degree of freedom vibration system, respectively, and $f(t)$ is the external excitation. For conciseness, let $x=x(t)$, $\dot{x}(t)=\dot{x}$, and $\ddot{x}(t)=\ddot{x}$.

On one hand, we define the initial conditions as $x_0=x(0)$, $v_0=\dot{x}(0)$. From the view of information processing, x is the output variable and $f(t)$ is the input variable. Considering the impulse response method, the solution of Eq. (1) can be calculated as

$$\begin{aligned} x = & \int_0^t f(\tau)\sin[\omega_{\rm d}(t-\tau)]\exp[-\xi\omega_{\rm n}(t-\tau)]\frac{{\rm d}\tau}{m\omega_{\rm d}} \\ & + v_0\sin(\omega_{\rm d}t)\frac{\exp[-\xi\omega_{\rm n}(t)]}{\omega_{\rm d}} \\ & + \frac{x_0\cos(\omega_{\rm d}t-\varphi)\exp[-\xi\omega_{\rm n}(t)]}{\sqrt{1-\xi^2}}, \end{aligned} \tag{2}$$

where $\omega_{\rm n}=\sqrt{k/m}$ is the natural frequency of the system, $\xi=c/2m\omega_{\rm n}$ is the damping rate, $\omega_{\rm d}=\omega_{\rm n}\sqrt{1-\xi^2}$ is the damping natural frequency and $\varphi=\arctan[(v_0+\xi\omega_{\rm n}x_0)/\omega_{\rm d}x_0]$.

It is apparent that finding parameter combinations including m, c, and k to filter $f(t)$ is quite hard in the general case, especially when the frequency of $f(t)$ is uncertain. In view of this problem, we rewrite Eq. (1) as follows:

$$\ddot{x}+p\dot{x}+qx-qs=0, \tag{3}$$

where $p=c/m$, $q=k/m$, and $s=f(t)/k$. Then, equation (3) can be changed into the form of a first-order differential equation set as

$$\begin{cases} \dot{x}=y, \\ \dot{y}=qs-qx-py, \end{cases} \tag{4}$$

where x represents the displacement response and y represents the velocity response from the view of vibration.

On the other hand, we can rewrite the forms of x and y as follows:

$$\begin{cases} x_{n+1}=x_n+\Delta x_n, \\ y_{n+1}=y_n+\Delta y_n, \end{cases} \tag{5}$$

where Δx_n and Δy_n represent the incremental values of x and y, respectively, $n\in{\rm N}$ and N represents the set of nonnegative integers. Denote the sampling instant t_n with $t_0=0$ and $t_0<t_1<t_2<\cdots<t_n$. Calculating the numerical solution of Eq. (5) by the second-order Euler method yields

$$\begin{cases} K_1=y_n, \\ K_2=y_n+hM_1, \\ M_1=qs_n-qx_n-py_n, \\ M_2=qs_n-qx_n-py_n-hK_1-hM_1, \end{cases} \tag{6}$$

where $h>0$ is the step size of the second-order Euler method, s_n is defined as the signal obtained by the n-th sampling. Then, we can obtain

$$\begin{cases} \Delta x_n=h(K_1+K_2)/2, \\ \Delta y_n=h(M_1+M_2)/2. \end{cases} \tag{7}$$

Note that the second-order Euler method is used to simplify the computational complexity of the filtering algorithm compared with the fourth-order Runge–Kutta method in Ref. [25].

Then, the short-term plasticity working model of a biological neuron in Ref. [24], which shows the convergence of facilitation and depression for the generation of a biological temporal filter, is considered. There exists an information segment exchange process; the temporal filtering functions appear to be derived from the interplay of particular combinations of short-term synaptic facilitation and depression.[23,24] Thus, we assume that Δx_n and Δy_n are information segments carried by biological neurons and that the values and parameters are dimensionless. According to the temporal filtering mechanism of biological neurons, Δx_n and Δy_n in Eq. (5) can be exchanged. It yields

$$\begin{cases} x_{n+1} = x_n + \Delta y_n, \\ y_{n+1} = y_n + \Delta x_n. \end{cases} \tag{8}$$

Substituting Eqs. (6) and (7) into Eq. (8), equation (8) results into the recursive equation, such that

$$\begin{pmatrix} x_{n+1} \\ y_{n+1} \end{pmatrix} = \begin{pmatrix} 1-qh\left(1-\dfrac{ph}{2}\right) & ph\left(1-\dfrac{ph}{2}\right)+\dfrac{qh^2}{2} \\ -\dfrac{qh^2}{2} & 1+h\left(1-\dfrac{ph}{2}\right) \end{pmatrix} \times \begin{pmatrix} x_n \\ y_n \end{pmatrix} + \boldsymbol{s}_{n+j+1} \begin{pmatrix} qh\left(1-\dfrac{ph}{2}\right) \\ \dfrac{qh^2}{2} \end{pmatrix}, \tag{9}$$

where $\boldsymbol{s}_{n+j+1}$ represents the input signal and j represents the number of signals delayed in the theory of filter. Simply, we define $a = -qh^2/2$, $b = h - ph^2/2$. Then, equation (9) yields

$$\boldsymbol{X}_i = \begin{pmatrix} 1-qb & a-pb \\ a & 1+b \end{pmatrix} \boldsymbol{X}_{i-1} + \boldsymbol{s}_{i+j} \begin{pmatrix} qb \\ -a \end{pmatrix}, \tag{10}$$

where $\boldsymbol{X}_i = (x_i, y_i)^{\mathrm{T}}$ is a 2×1 state vector, $i \in N^+$ and N^+ represent the set of positive integers. Equation (10) is the kernel equation of the developed fast filtering algorithm.

2.2. Parameter analysis

With reference to the initial value selection, apparently $\boldsymbol{X}_0$ exists in several different conditions, such as single value (no signal delay, $j=0$), double value (one signal delay, $j=1$), trio value (two signal delay, $j=2$), etc. Here, we take into account the double value condition to discuss the features of the developed fast filtering algorithm. In this case, the recursive function can be written as follows:

$$\begin{cases} \boldsymbol{X}_0 = \begin{pmatrix} 1-\alpha & \alpha \\ -1 & 1 \end{pmatrix} \begin{pmatrix} s_0 \\ s_1 \end{pmatrix}, \\ \boldsymbol{X}_i = \begin{pmatrix} 1-qb & a-pb \\ a & 1+b \end{pmatrix} \boldsymbol{X}_{i-1} + \boldsymbol{s}_{i+1} \begin{pmatrix} qb \\ -a \end{pmatrix}, \end{cases} \tag{11}$$

where $\alpha \in [0,1]$ denotes the total input coefficient of signals. Then, we define $\boldsymbol{A}$ and $\boldsymbol{B}$ as follows:

$$\boldsymbol{A} = \begin{pmatrix} 1-qb & a-pb \\ a & 1+b \end{pmatrix}, \quad \boldsymbol{B} = \begin{pmatrix} qb \\ -a \end{pmatrix}. \tag{12}$$

Considering the recursive process and substituting Eq. (12) into Eq. (11), we have

$$\begin{cases} \boldsymbol{X}_0 = s_0 \begin{pmatrix} 1-\alpha \\ -1 \end{pmatrix} + s_1 \begin{pmatrix} \alpha \\ 1 \end{pmatrix}, \\ \boldsymbol{X}_i = \boldsymbol{A}^i \boldsymbol{X}_0 + \sum_{l=0}^{i-1} \boldsymbol{s}_{i+1-l} \boldsymbol{A}^l \boldsymbol{B}, \end{cases} \tag{13}$$

where $\boldsymbol{X}_i = (x_i, y_i)^{\mathrm{T}}$ and $i \in N^+$.

We define the expansion coefficients of x_i and y_i as δ_i and η_i, respectively. Then, the main results of the parameter analysis are given in the following theorem and inferences.

Theorem 1 For any $i \in N^+$, $\sum \delta_i = 1$, and $\sum \eta_i = 0$. The sums of expansion coefficients regarding x_i and y_i are irrelevant to the delayed number j.

Proof of theorem Firstly, we take into account $j=1$. In this case, when $i=1$, the expansion coefficients can be written as follows:

$$\begin{pmatrix} \delta_1 \\ \eta_1 \end{pmatrix} = \begin{pmatrix} 1 \\ 0 \end{pmatrix}.$$

Assume that the theorem is true when $i=n$ and $n \in N^+$. Then

$$\begin{pmatrix} \sum \delta_n \\ \sum \eta_n \end{pmatrix} = \boldsymbol{A}^n \left[\begin{pmatrix} 1-\alpha \\ -1 \end{pmatrix} + \begin{pmatrix} \alpha \\ 1 \end{pmatrix} \right] + \sum_{l=0}^{n-1} \boldsymbol{A}^l \boldsymbol{B} = \begin{pmatrix} 1 \\ 0 \end{pmatrix}.$$

Thus, when $i = n+1$, we can obtain

$$\begin{aligned} \begin{pmatrix} \sum \delta_{n+1} \\ \sum \eta_{n+1} \end{pmatrix} &= \boldsymbol{A} \begin{pmatrix} \sum \delta_n \\ \sum \eta_n \end{pmatrix} + \boldsymbol{B} \\ &= \begin{pmatrix} 1-qb & a-pb \\ a & 1+b \end{pmatrix} \begin{pmatrix} 1 \\ 0 \end{pmatrix} + \begin{pmatrix} qb \\ 1-a \end{pmatrix} \\ &= \begin{pmatrix} 1 \\ 0 \end{pmatrix}. \end{aligned}$$

Obviously, the delayed number j has nothing to do with the process of proof. Thus, we can obtain that: no matter how many numbers the signals delay, the theorem is always tenable.

Inference 1 For any $i \in N^+$, $\sum \delta_i = 1$ and $\sum \eta_i = 0$, x_i can be seen as a linear combination similar to the points in space and y_i can be seen as a different linearity, such as the feature of the vector. In this case, we can consider that x_i is a signal value and y_i is an incremental value.

Inference 2 Considering Eq. (13), the parameters of $\boldsymbol{s}$ need to meet $\boldsymbol{X}_i$. Different parameter combinations provide different filtering types, e.g., if all parameters are positive and one of them is much greater than the others while it is close to 1, equation (11) can be used for low-pass filtering; if one positive item is much larger and others show absolutely small

values, as well as negative items existing, equation (11) can realize the high-pass filtering process.

Remark 1 For the derivation of Eq. (10), the following parameter conditions should be satisfied

$$\begin{cases} h > 0, \\ q > 0, \\ p + \alpha qh < 2(h+\alpha)/h, \\ p - (1-\alpha)qh > 2(h+\alpha-1)/h. \end{cases} \tag{14}$$

Moreover, the fluctuation parameter space is partitioned by the following equation set

$$\begin{cases} f_1(p,q,h) = h = 0, \\ f_2(p,q,h) = q = 0, \\ f_3(p,q,h) = 2(h+\alpha) - ph - \alpha qh^2 = 0, \\ f_3(p,q,h) = 2(h+\alpha-1) + (1-\alpha)qh^2 - ph = 0. \end{cases} \tag{15}$$

Different subspaces of parameter combinations based on frequency selective filtering are given by Eq. (15); the implemented law depends on Eq. (14).

Remark 2 From a mathematics point of view, equation (11) has a certain filtering property while it fulfills the conditions of Eq. (14). However, not all the parameters which satisfy Eq. (11) can fulfill Eq. (14). Therefore, equation (14) indicates the sufficient condition, but that it is an unnecessary condition with regard to Eq. (11).

Remark 3 By Eq. (15), different parameter combinations can be selected according to different features of signals that need to be filtered. In a sense, it indicates that equation (10) shows an adaptive ability, which can be used for further research.

Remark 4 A feasible optimized parameter criterion under the minimum error variance condition is given as follows:

$$-q^3h^4 + 4q^2(h+1) - 4q(h+2) + 4 = 0. \tag{16}$$

The corresponding derivation can be seen in the Appendix. According to Eqs. (14)–(16), the acceptable parameter combinations can be selected.

3. Experiments and discussion

To verify the feasibility and the superiority of the proposed fast filtering algorithm in Eq. (10), firstly, we compare the filtering performances of some typical signals and the computation time of actual signals by various filtering algorithms. Then, we apply it to the navigation and positioning system of the micro motion robot for further illustration.

3.1. Filtering performance comparison by various filtering methods

In this subsection, the single degree of freedom vibration system filtering algorithm referred to in Ref. [25] is denoted as method I, the proposed fast filtering algorithm is denoted as method II, the FWT algorithm, method III and the particle method, method IV. Considering Eqs. (14) and (15), two different parameter combinations are given in Table 1; the corresponding relationships between amplitude and frequency for proposed fast filtering algorithm are shown in Fig. 1, where the dash line represents the characteristics of band-pass filtering which passband is approximately from 40 Hz to 180 Hz. The solid line represents the characteristics of low-pass filtering which passband is approximately under 180 Hz.

Table 1 . The select parameter combinations.

Parameter combinations	p	q	α	h
I	0.2	0.1	0.7	0.2
II	0.9	0.2	0.7	0.3

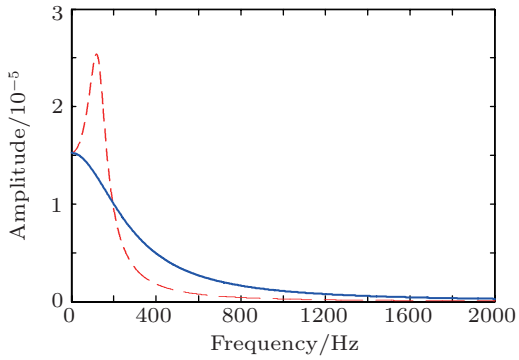


Fig. 1. (color online) Amplitude-frequency curves for the proposed fast filtering algorithm based on Table 1.

On one hand, we adopt four groups of typical signals, the sawtooth signal, the sawtooth signal with sinusoidal, the square signal and the square signal with sawtooth. The frequency band of these four typical signals is from 1 Hz to 20 Hz. The adopted sampling frequency is 1000 Hz and the noise is 10 dB white noise. In Fig. 1, apparently the low-pass filtering is suitable for the four typical signals. The comparisons among method I, II, III, and IV are given by simulation and numerical testification. The comparison results can be seen in Fig. 2, where the first row shows the original signals, the second row shows the adding noise signals, the third row shows the signals filtered by method I, the fourth shows the signals filtered by method II, the fifth shows the signals filtered by method III and the last shows the signals filtered by method IV. As illustrated in Fig. 2, for the four typical signals with white noise, the filtering results of method II are better than that of methods I, III, and IV. For instance, the outputs of method II are much smoother than others. It indicates that the proposed fast filtering algorithm demonstrates a better denoising capability compared with the other three filtering methods. Moreover, the numerical testifications including signal noise ratio (SNR/dB), root mean square error (RMSE) and signal noise ratio gain (SNRG) are carefully evaluated to compare

method I, II, III, and IV. The comparison results of numerical testifications are shown in Table 2. For further analysis of the data in Table 2, let $I_S(k) = (S_{II} - S_k)/S_k \times 100\%$, $I_R(k) = (R_{II} - R_k)/R_k \times 100\%$, $I_G(k) = (G_{II} - G_k)/G_k \times 100\%$, where S_k, R_k, G_k, $\forall k = I, III, IIV$, represent SNR, RMSE, SNRG, respectively, for the four cases of filtering methods, i.e., the single degree of freedom vibration system filtering algorithm, the proposed fast filtering algorithm, the FWT algorithm and the particle filtering method. The results are shown in Table 3. The data of Tables 2 and 3 directly demonstrate that SNR and SNRG of method II show improvement while the corresponding RMSE reduces compared with method I, III and IV. It proves that the proposed fast filtering algorithm is superior to the other three filtering methods.

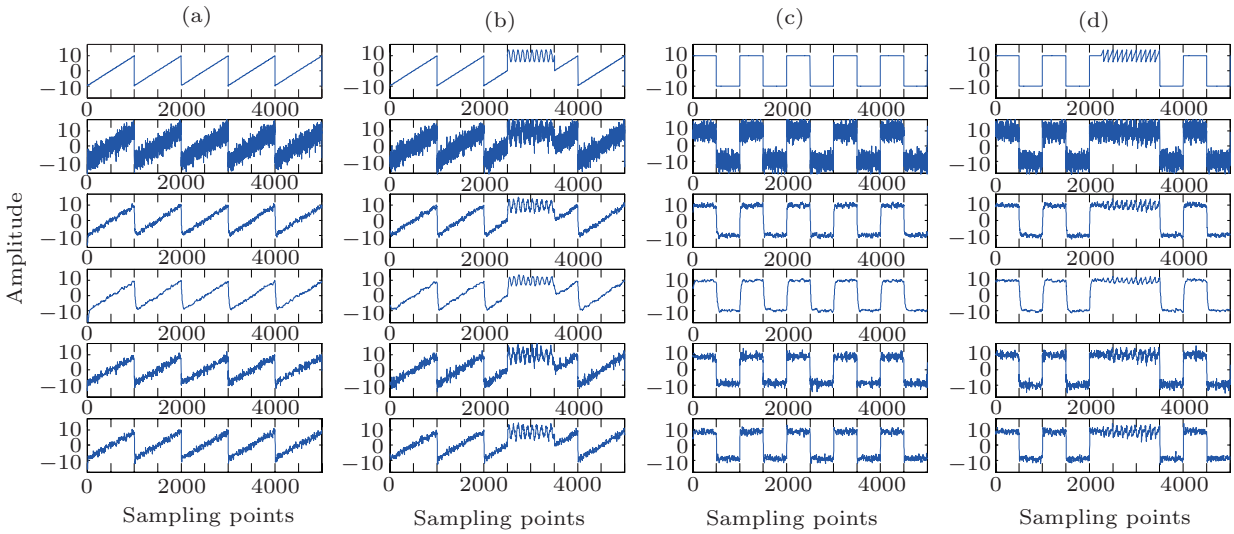


Fig. 2. (color online) Comparisons of various filtering methods. From top to bottom: the first row represents the original typical signals whose frequencies are from 1 Hz to 20 Hz; the second row represents the typical signals with 10-dB white noise; the third row represents the filtering results obtained by method I; the fourth row represents the filtering results obtained by method II; the fifth row represents the filtering results obtained by method III; and the last row represents the filtering results obtained by method IV. The horizontal coordinates represent the sampling points and the vertical coordinates represent the signal sizes.

Table 2. Performance comparisons of various filtering methods.

Typical signals	Filtering method	SNR/ dB	RMSE	SNRG
Sawtooth	I	34.3	0.0079637	3.3015
	II	39.231	0.0058991	3.7762
	III	30.381	0.010133	2.9243
	IV	27.713	0.012019	2.6675
Sawtooth with sinusoidal	I	38.242	0.0075866	2.8396
	II	45.56	0.0048683	3.3829
	III	32.711	0.010716	2.4289
	IV	31.875	0.011325	2.3668
Square	I	43.416	0.0080982	2.1675
	II	46.815	0.0065347	2.3371
	III	38.347	0.010993	1.9144
	IV	36.816	0.012087	1.8379
Square with sawtooth	I	44.019	0.0079114	2.1887
	II	50.639	0.0053147	2.5178
	III	38.673	0.010938	1.9229
	IV	37.696	0.011656	1.8743

On the other hand, the proposed fast filtering algorithm is testified in the advanced reduced instruction set computing machines (ARM7:LPC2148). The main frequency is 60 MHz and the sampling points are 3500. Firstly, to illustrate the feasibilities of method I, II, III, and IV for actual signals, two different electrocardiogram (ECG) signals are filtered respectively according to Fig. 1 and Table 1. The filtering results of the four filtering methods are shown in Fig. 3. The first row of Fig. 3 represents the original ECG signals; the second represents the signals filtered by method I; the third represents the signals filtered by method II; the fourth represents the signals filtered by method III; and the last represents the signals fil-

tered by method IV. The four filtering methods can obtain the whole waveform of ECG signals. The ECG signal feature can be seen clearly. Thus, the four filtering methods can be applied to ARM7. The computation time of method I, II, III, and IV are obtained as shown in Table 4. The data in Table 4 illustrates that, under the same conditions, the computation time of method I, method III and method IV are approximately 1.2, 77.7, and 61 times than that of method II.

Table 3. Computation results of I_S, I_R, I_G according to the data in Table 2.

Typical signals	Filtering method	$I_S(k)$	$I_R(k)$	$I_G(k)$
Sawtooth	I	+14.376	–25.925	+14.378
	III	+29.13	–41.783	+29.131
	IV	+41.562	–50.918	+41.563
Sawtooth with sinusoidal	I	+19.136	–35.83	+19.133
	III	+39.28	–54.57	+39.277
	IV	+42.933	–57.013	+42.931
Square	I	+7.829	–19.307	+7.825
	III	+22.083	–40.556	+22.080
	IV	+27.159	–45.936	+27.161
Square with sawtooth	I	+15.039	–32.822	+15.036
	III	+30.941	–51.411	+30.938
	IV	+34.335	–54.404	+34.333

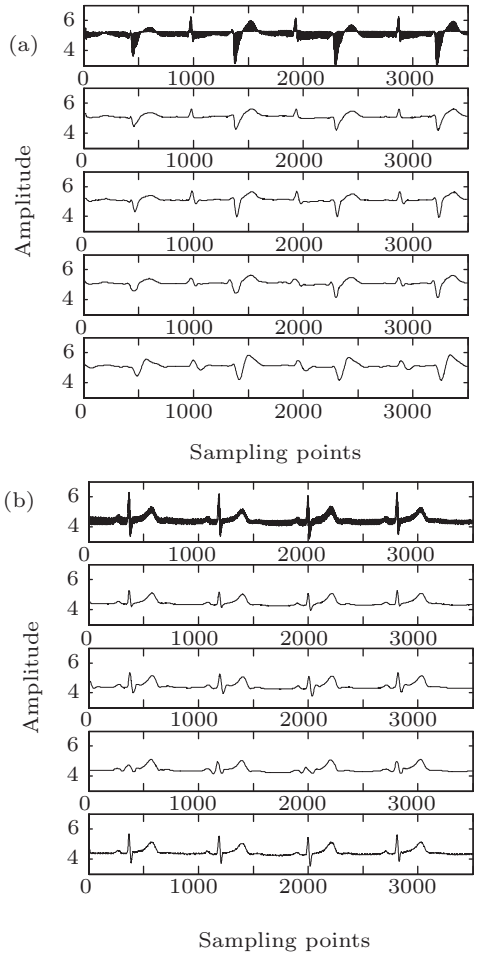


Fig. 3. Comparisons of various filtering methods for different ECG signals. From top to bottom: the first row represents the measured ECG signals; the second row represents the filtering results obtained by method I; the third row represents the filtering results obtained by method II; the fourth row represents the filtering results obtained by method III; and the last row represents the filtering results obtained by method IV. The horizontal coordinates represent the sampling points and the vertical coordinates represent the signal sizes.

Table 4. The computation time (millisecond).

Filtering method	I	II	III	IV
Computation time	0.88	0.73	56.7	44.5

With the foregoing discussion, the comparisons indicate that the efficiency of the proposed fast filtering algorithm is further improved than that of the single degree of freedom vibration system filtering algorithm. Not only that, but the computation time is far less than that of the FWT algorithm and the particle method. Consequently, the proposed fast filtering algorithm shows a higher filtering speed and better filtering performance and is more suitable towards high real-time processing scenarios. Therefore, we shall testify its application on the navigation and positioning system of the micro motion robot, which needs an extremely high real-time requirement in the next subsection.

3.2. Testification on navigation and positioning system of the micro motion robot

The micro motion robot driven by double crawlers shown in Fig. 4 is 240 mm×220 mm×68 mm. The hardware composition of its navigation and positioning system is shown in Fig. 5. A Chinese coin, whose diameter is 10 mm, is placed next to the hardware system as a reference scale. Note that the working environment determines the unique characteristics of the micro motion robot. It is demanded that the micro motion robot should run stable and have high real-time information processing ability. In this case, the navigation and positioning system of the micro motion robot is generally composed of the following two subsystems.

(I) Electrocircuit subsystem. This subsystem contains the power supply, complex programmable logic device (CPLD)

and micro-electromechanical systems (MEMS) kernel electrocircuit.

(II) Passivity wheel subsystem. The photoelectric coder is embedded in this subsystem.

The MEMS kernel electrocircuit is of great importance in the navigation and positioning system of the micro motion robot for the estimation of the heading and the attitude. In the electrocircuit subsystem, the MEMS devices contain the accelerometer and the gyro. The microprocessor of the micro motion robot adopts ARM7:LPC2148 and its main frequency is 60 MHz. The MEMS accelerometer adopts ADIS16201 and the MEMS gyro adopts ADIS16255. The sampling frequency is 1000 Hz.

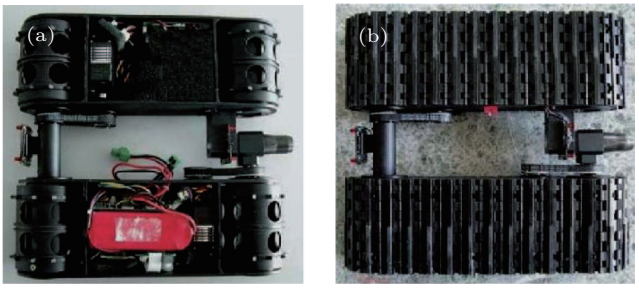


Fig. 4. (color online) The micro motion robot (a) before and (b) after tracks are installed.

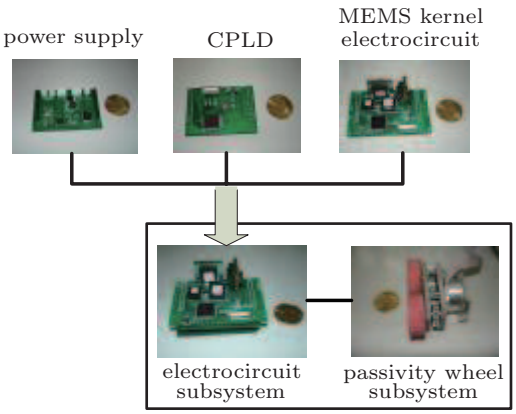


Fig. 5. (color online) Hardware composition of the navigation and positioning system in the micro motion robot.

3.2.1. Signal preprocessing

The filtering processes of measured accelerometer signals and gyro signals can be seen as the signal preprocessing process in the navigation and positioning system of the micro motion robot. The preprocessing results can be used to estimate the heading and the attitude of the micro motion robot. In this subsection, the proposed fast filtering algorithm is applied to signal preprocessing for its high filtering speed, which can meet the high real-time information processing ability of the micro motion robot efficiently.

3.2.1.1. Accelerometer signals filtering

The measured accelerometer signals with the sample points of 2000 are illustrated in the top of Fig. 6, where figures 6(a) and 6(b) represent the dynamic and the static measured signals in the accelerometer, respectively. As shown in Fig. 6, the measured original signals in the accelerometer are disturbed by random noise whose intensity is almost the same as the useful signals. According to the features of the dynamic and the static measured signals in the accelerometer, the frequency of dynamic measured signals is approximately 5 Hz and the static measured signals, which are mainly produced by the natural vibration of the micro motion robot, should obtain an amplitude balance in quite a small range to guarantee that the micro motion robot runs stable. In this case, the developed fast filtering algorithm is applied to filter the measured accelerometer signals; the parameter combination method II in Table 1 can be used according to the relationship between amplitude and frequency in Fig. 1.

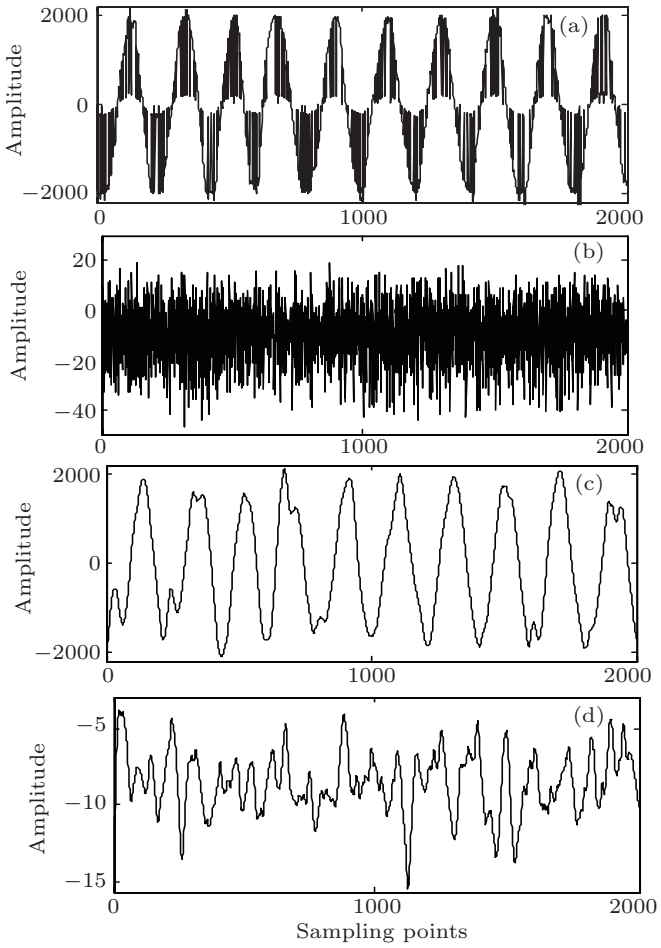


Fig. 6. The signals of the accelerometer. Left, from top to bottom: panel (a) represents the dynamic measured signals in the accelerometer; panel (c) represents the filtering result of the dynamic signals. Right, from top to bottom: panel (b) represents the static measured signals in the accelerometer; panel (d) represents the filtering result of the static signals. The horizontal coordinates represent the sampling points and the vertical coordinates represent the signal sizes.

In Fig. 6, figures 6(c) and 6(d) represent the filtering results of the dynamic and the static signals in the accelerometer by the developed fast filtering algorithm, respectively. Apparently, the high frequency noises superimposed on the measured accelerometer signals have already been removed to a

great extent. It indicates that the developed fast filtering algorithm can filter the measured accelerometer signals effectively. However, the filtering performance of static measured accelerometer signals, as shown in Fig. 6(d), is not very good. Its amplitude range is approximately from −15 to −6. It is too large to produce a great error. Hence, a second-level filtering method is considered to address this problem.

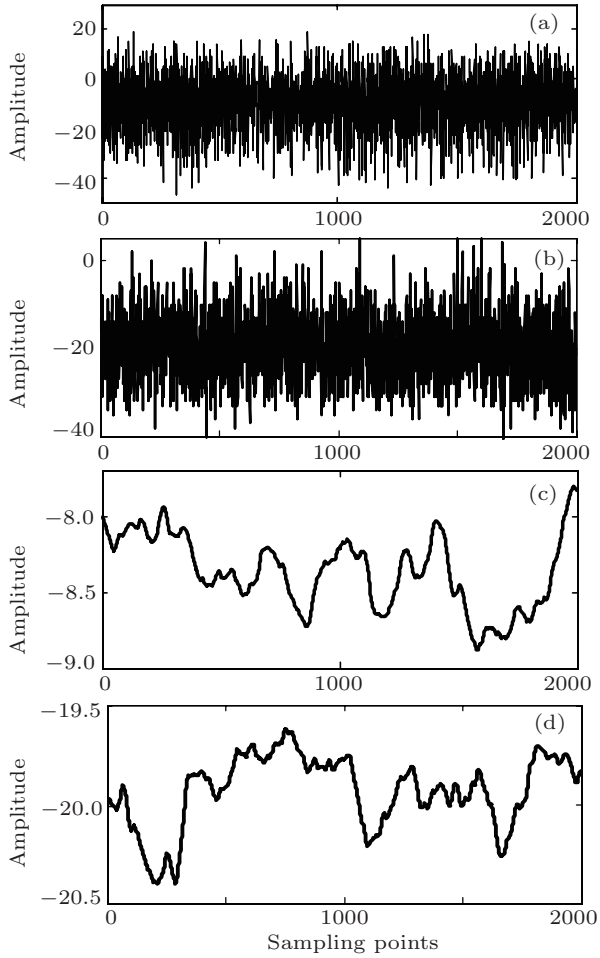


Fig. 7. The second-level filtering processes. Left, from top to bottom: panel (a) represents the static measured signals in the accelerometer; panel (c) is for the second-level filtering result of panel (a). Right, from top to bottom: panel (b) represents the static measured signals in the gyro; panel (d) is for the second-level filtering result of panel (b). The horizontal coordinates represent the sampling points and the vertical coordinates represent the signal sizes.

The second-level filtering method means to filter the outputs of the developed fast filtering algorithm under the same conditions once again. Theoretically, the outputs should be computed by Eq. (10) with the same parameter combinations again. The simulation results of the second-level filtering method are shown in Fig. 7. In Fig. 7(c), the amplitude range of static measured accelerometer signals shows a further decrease after the second-level filtering process. It is approximately from −8.8 to −7.8. Thus, the static measured accelerometer signals are approximately stable. From the foregoing, we can obtain that, if the frequency range of the original signals is certain, the superimposed noise can be filtered by the developed fast filtering algorithm; besides, combined with the real motion of the micro motion robot, if the filtered signals are not suitable for the requirements, we still need to consider the second-level filtering method for better performance. Furthermore, if the filtering results are still inappropriate, a higher-level filtering process can be taken into account.

3.2.1.2. Gyro signals filtering

The measured gyro signals are sampled under the same condition as the measured accelerometer signals. As shown in the first row of Fig. 8, figure 8(a) shows the dynamic measured gyro signals, and figure 8(b) shows the static measured gyro signals. The frequency of dynamic measured gyro signals is approximately 15 Hz; the static measured gyro signals need to obtain an amplitude balance similar to the static measured accelerometer signals. The filtering results are shown in the second row of Fig. 8, where Figs. 8(c) and 8(d) show the dynamic and the static measured gyro signals filtered by the developed fast filtering algorithm, respectively.

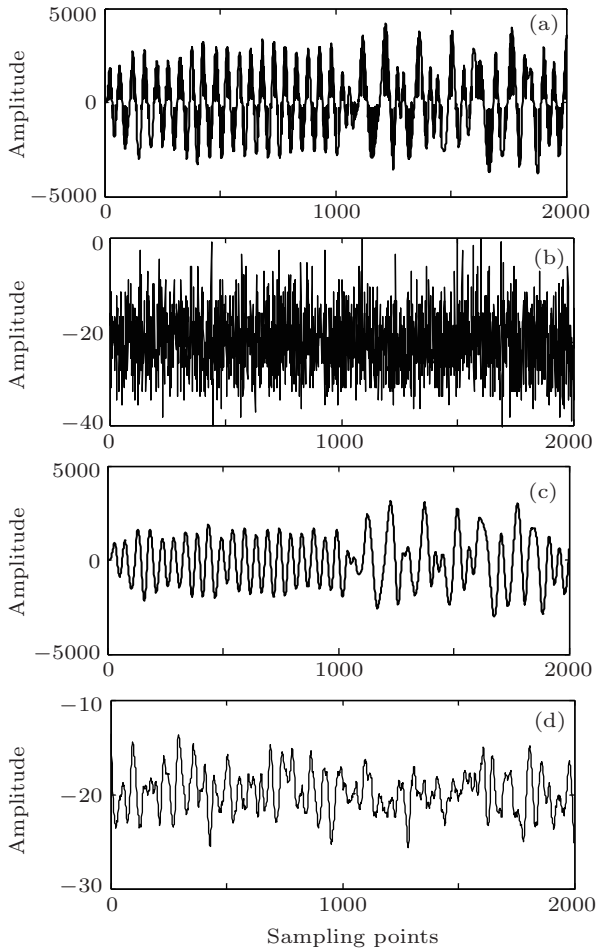


Fig. 8. The signals of the gyro. Left, from top to bottom: panel (a) represents the dynamic measured signals in the gyro; panel (c) represents the low-pass filtering result of the dynamic signals. Right, from top to bottom: panel (b) represents the static measured signals in the gyro; panel (d) represents the low-pass filtering result of the static signals. The horizontal coordinates represent the sampling points and the vertical coordinates represent the signal sizes.

In Fig. 8, the filtering performances of dynamic and static measured gyro signals are similar to those of accelerometer

signals; the noise superimposed on measured gyro signals is removed effectively. As shown in Fig. 8(c), the dynamic measured gyro signals are filtered well; the filtering results can be applied to the motion estimation of the micro motion robot. However, in the case of the static measured gyro signals, as shown in Fig. 8(d), the amplitude range of filtering results is approximately from −25 to −15. It is not a satisfactory result for the micro motion robot. Hence, considering the second-level filtering method, the amplitude range changes. As shown in Fig. 7(d), it is approximately from −20.4 to −19.7, while the static measured gyro signals are approximately stable.

3.2.2. Estimation of heading error and attitude error for micro motion robot based on signal preprocessing

The signal preprocessing results obtained in the previous subsection can be used as the navigation and positioning data of the micro motion robot. By communication with the robot controller, the motion state and the attitude information of the micro motion robot can be estimated according to the navigation and positioning data. Hence, taking into account the navigation and positioning system shown in Fig. 5, we propose two sets of experiments for estimating the heading angle error and the attitude angle error, respectively, by the signal preprocessing results to verify the efficiency of the developed fast filtering algorithm in high real-time requirement systems. On one hand, for the heading angle error, the experimental process comprises the following steps.

Step 1 Make the micro motion robot to be stationary on a rigid horizontal plane. After calibrating, define the original heading angle as 0. Then, define the coordinate system of the micro motion robot.

Step 2 Control the micro motion robot to rotate around the z axis. Limit the rotation angle by a location mark. After turning 360°, the micro motion robot returns *in situ*. The time and the radius of each rotation are approximately 60 s and 300 mm, respectively.

Step 3 Repeat step 1 and step 2 10 times. In order to obtain more randomness in experimental results, the micro motion robot is controlled to rotate around the z axis in clockwise and anticlockwise directions, respectively, 5 times in each direction.

The experimental results are listed in Table 5; the average value is also given. Moveover, the histogram is used to illustrate the estimated results of heading angle error. As shown in Fig. 9, the data from the serial number 1 to 10 represent the experimental results, and that of serial number 11 represents the average estimated value. The micro motion robot produces 2° heading angle errors per revolution on average. Generally, the heading angle error is low enough to reach the requirements of the micro motion robot. The heading angle error in this experiment is caused for two reasons: firstly, due to the relativity of the horizontal plane, the plane still exists slightly irregular; secondly, the micro motion robot vibrates naturally in the rotation process.

Table 5. Experimental results of heading angle error estimation.

Serial number	Heading angle error/(°)
1 (Clockwise)	1.7
2 (Clockwise)	2.6
3 (Clockwise)	2.3
4 (Clockwise)	2.0
5 (Clockwise)	2.9
6 (Anticlockwise)	2.1
7 (Anticlockwise)	2.6
8 (Anticlockwise)	1.8
9 (Anticlockwise)	2.4
10 (Anticlockwise)	2.3
11 (Average value)	2.0

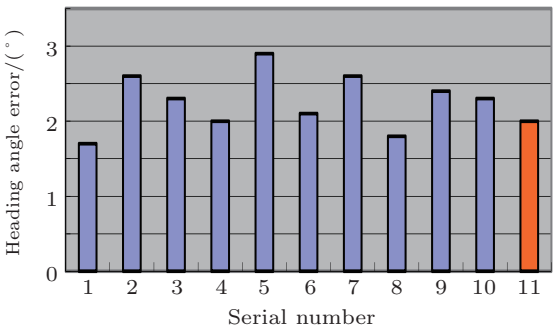


Fig. 9. (color online) The experimental histogram of heading angle error estimation.

On the other hand, for the attitude angle error, it is tested on a slope whose angle is 35° with the rigid horizontal plane. The process is shown as the following steps.

Step i Make the micro motion robot stationary on the horizontal plane. After calibrating, define the original pitch angle as 0.

Step ii Control the micro motion robot to move to-and-fro along the slope. Repeat the movement 10 times, so each to-and-fro movement lasts 60 seconds. Record the value of the pitch angle each time.

The experimental results are shown in Table 6. The average value is also calculated. Then, the histogram is used to illustrate the estimated results of attitude angle error. As shown in Fig. 10, the data from the serial numbers 1 to 10 represent the experimental results, while that of serial number 11 represents the average estimated value. Obviously, the attitude angle error is quite small; its average value is 0.9. It indicates that the estimated accuracy is quite good.

The experiments conducted above (described in Section 3) show the simulation analysis and practical application

of the developed fast filtering algorithm. Two advantages are illustrated in this section: firstly, the developed fast filtering algorithm performs better than the single degree of freedom vibration system filtering algorithm, the FWT algorithm, and the particle filtering method, especially in the filtering time and performance; secondly, the developed fast filtering algorithm can be effectively used for the high real-time requirement systems, e.g., in the navigation and positioning system of the micro motion robot.

Table 6. Experimental results of attitude angle error estimation.

Serial number	Attitude angle error/(°)
1	0.7
2	1.0
3	1.1
4	0.9
5	1.2
6	0.6
7	0.7
8	0.8
9	1.1
10	0.7
11 (Average value)	0.9

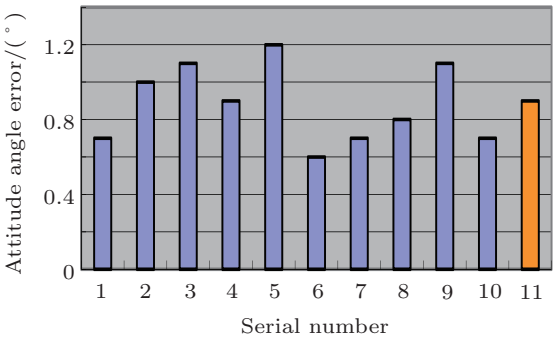


Fig. 10. (color online) The experimental histogram of attitude angle error estimation.

4. Conclusions

We present a developed fast filtering algorithm based on vibration systems and neural information exchange, tested by simulation and practical approaches, then applied to the navigation and positioning system of the micro motion robot, which is of high real-time requirement. The characters including derivation process and parameter analysis are discussed. The filtering performances including numerical verification, such as SNR, RMSE and SNRG, and computing time are carefully compared among different filtering algorithms; the superiorities of the proposed fast filtering algorithm are shown by the comparisons. Then, according to the extremely high filtering speed, the proposed fast filtering algorithm can meet the high real-time requirement of the navigation and positioning system in the micro motion robot; its effectiveness is further testified by the estimation experiments of the heading angle error and the attitude angle error for the micro motion robot.

Appendix A

Considering the complete filtering and observation process for Eq. (10), it yields

$$\begin{cases} \boldsymbol{X}_i = \boldsymbol{A}\boldsymbol{X}_{i-1} + \boldsymbol{B}\boldsymbol{s}_{i+j}, \\ \boldsymbol{Z}_i = \boldsymbol{H}\boldsymbol{X}_i + \boldsymbol{V}_i, \end{cases} \tag{A1}$$

where $\boldsymbol{X}_i$ represents the input sequence, $\boldsymbol{Z}_i$ represents the observing sequence, $\boldsymbol{A}$ and $\boldsymbol{B}$ are the parameter matrixes, $\boldsymbol{H} = [1\ \ 0]$ is the observing matrix, $\boldsymbol{V}_i$ represents the white noise caused by observation equipment with the expectation $\mathrm{E}[\boldsymbol{V}_i] = 0$ and the variance value $\sigma[\boldsymbol{V}_i] = r$.

Denote the predicted state sequence as $\boldsymbol{P}_i$, the predicted observing sequence as $\boldsymbol{Q}_i$. According to Eq. (A1), the step predicted equation of the filtering and observing process can be described as

$$\begin{cases} \boldsymbol{P}_{i,i-1} = \boldsymbol{A}\boldsymbol{P}_{i-1} + \boldsymbol{B}\boldsymbol{s}_{i+j}, \\ \boldsymbol{Q}_{i,i-1} = \boldsymbol{H}\boldsymbol{P}_{i,i-1}, \end{cases} \tag{A2}$$

where $\boldsymbol{P}_{i,i-1}$ is the step predicted state sequence and $\boldsymbol{Q}_{i,i-1}$ is the step observed sequence. Denote the state error as $\boldsymbol{D}_i$ and the observing error as $\boldsymbol{F}_i$, $\boldsymbol{D}_i = \boldsymbol{X}_i - \boldsymbol{P}_i$, $\boldsymbol{F}_i = \boldsymbol{Z}_i - \boldsymbol{Q}_i$. For $\boldsymbol{F}_i$ can be used to upgrade predicted state sequence $\boldsymbol{P}_i$ in a step predicted process, we have

$$\boldsymbol{P}_i = \boldsymbol{P}_{i,i-1} + \boldsymbol{F}_i. \tag{A3}$$

We define the error variance matrix as $\boldsymbol{J}_i$. While the filtering process is stable, the error variance is constant, i.e., $\boldsymbol{J}_i = \boldsymbol{J}$. The error variance matrix function can be described as follows:

$$\boldsymbol{J} = E[\boldsymbol{D}\boldsymbol{D}^{\mathrm{T}}], \tag{A4}$$

where $\boldsymbol{J}$ represents the minimum error variance matrix and $E[\cdot]$ represents the mathematic expectation. Considering Eqs. (A2) and (A3), minimizing the error variance matrix $\boldsymbol{J}$, we can obtain

$$\boldsymbol{J} = (\boldsymbol{I} - r^{-1}\boldsymbol{J})\boldsymbol{A}\boldsymbol{J}\boldsymbol{A}^{\mathrm{T}}, \tag{A5}$$

where r is the variance value of observation noise and $\boldsymbol{A}$ is the parameter matrix. Then, a feasible optimized parameter criterion under the minimum error variance condition is obtained according to the solution process of Eq. (A5).

$$-q^3h^4 + 4q^2(h+1) - 4q(h+2) + 4 = 0. \tag{A6}$$

References

[1] Hsia C H, Guo J M and Chiang J S 2012 *Signal Process.* **92** 89
[2] Leng H Z and Song J Q 2013 *Chin. Phys. B* **22** 030505
[3] Sheng Z, Chen J Q and Xu R H 2012 *Acta Phys. Sin.* **61** (in Chinese)
[4] Wu X D and Song Z H 2008 *Chin. Phys. B* **17** 3241
[5] Lefebvre A, Corpetti T and Moy L H 2011 *Pattern Recogn. Lett.* **32** 190
[6] Gustafsson F 2010 *IEEE Aerosp. Electron. Syst. Mag.* **25** 53
[7] Strang G 1989 *SIAM Rev.* **31** 614
[8] Cody M A 1992 *Dr. Dobbs J.* **17** 16
[9] Beylkin G, Coifman R and Rokhlin V 1991 *Commun. Pure Appl. Math.* **44** 141
[10] Grossmann A and Morlet J 1984 *SIAM J. Math. Anal.* **15** 723
[11] Gao G R, Liu Y P and Pan Q 2012 *Acta Phys. Sin.* **61** 139701 (in Chinese)
[12] Zhang L X and Boukas E K 2009 *Automatica* **45** 1462
[13] Zhang L X and Shi P 2011 *Int. J. Syst. Sci.* **42** 781
[14] Doucet A, Gordon N J and Krishnamurthy V 2001 *IEEE Trans. Signal Process.* **49** 613
[15] Mukherjee A and Sengupta A 2010 *Signal Process.* **90** 1873
[16] Arulampalam M S, Maskell S, Gordon N and Clapp T 2002 *IEEE Trans. Signal Process.* **50** 174
[17] Nishiyama K 2005 *Signal Process.* **85** 2412
[18] Leng H Z, Song J Q, Cao X Q and Yang J H 2012 *Acta Phys. Sin.* **61** 070501 (in Chinese)
[19] Thompson W T and Dahleh M D 1997 *Theory of Vibrations with Applications* (5th edn.) (New Jersey: Prentice Hall) p. 28
[20] Chen Z S and Yang Y M 2011 *Acta Phys. Sin.* **60** 074301 (in Chinese)
[21] Zhang J J and Jin Y F 2012 *Acta Phys. Sin.* **61** 130502 (in Chinese)
[22] Masuda N and Aihara K 2003 *Phys. Lett. A* **311** 485
[23] Horcholle-Bossavit G and Quenet B 2009 *Biosystems* **97** 35
[24] Forture E S and Rose G J 2001 *Trends Neurosci.* **24** 381
[25] Zha F S, Chen J X, Li M T, Guo W and Wang P F 2012 *Neurocomputing* **97** 1